Science Advances
AAAS

advances.sciencemag.org/cgi/content/full/5/7/eaax1081/DC1

Supplementary Materials for

Single molecule–mediated assembly of polyoxometalate single-cluster rings and their three-dimensional superstructures

Qingda Liu, Peilei He, Hongde Yu, Lin Gu, Bing Ni, Dong Wang*, Xun Wang*

*Corresponding author. Email: wangxun@mail.tsinghua.edu.cn (X.W.); dong913@mail.tsinghua.edu.cn (D.W.)

Published 26 July 2019, *Sci. Adv.* **5**, eaax1081 (2019)
DOI: 10.1126/sciadv.aax1081

This PDF file includes:

Supplementary Materials and Methods

Materials:
Octadecyltrimethylammonium bromide (OTAB, ≥99.0%), cetyltrimethylammonium bromide (CTAB, ≥99.0%), tetradecyltrimethylammonium bromide (TTAB, ≥99.0%), dodecyltrimethylammonium bromide (DTAB, ≥99.0%) and tetrabutylammonium bromide (TBAB, ≥99.0%) were purchased from sinopharm. All reagents were used as purchased without further purification.

A series of $P_2W_{17}M$ clusters, containing $K_7P_2W_{17}LnO_{61}$ (*33*) (Ln = La, Ce, Pr, Nd, Sm, Eu, Gd), $K_8P_2W_{17}TiO_{61}$ (*34*), $K_7P_2W_{17}VO_{62}$ (*35*), $K_7P_2W_{17}CrO_{61}$ (*36*), $K_8P_2W_{17}MnO_{61}$ (*37*), $K_8P_2W_{17}CoO_{61}$, $K_8P_2W_{17}NiO_{61}$, $K_8P_2W_{17}CuO_{61}$ (*38*), $K_8P_2W_{17}ZnO_{61}$ (*39*) were prepared following the literature and were employed as building blocks.

Methods:
General procedure for olefin epoxidation reaction:
Olefin (30 μmol), 5.5 mg of $P_2W_{17}Mn$ nanowire and 20 mg of PhIO were added into 1 mL CH_3CN. The reaction was performed at 30 ℃ for 2 hours under continuous magnetic stirring. Finally, the solution was centrifuged and the supernatant was studied by chromatography. In the control experiment, same molar ratio of $P_2W_{17}Mn$ POM precursor was employed and the reaction time was prolonged to 5 h.

Electrochemistry experiments:
CV and amperometric measurements were performed on a CHI660D electrochemical workstation. A standard three-electrode cell was used during the experiment. SCE(saturated calomel electrode) and platinum wire were used as reference and counter electrode.

Detection of Hydrogen Peroxide:
The POM 3D superstructures were dispersed in chloroform with a concentration of 8 mg mL^{-1}. 4 μL of solution was dropped on the surface of glass carbon electrodes (diameter 5 mm). Then 2 μL of Nafion solution (0.5% in ethanol) was dropped on the sample and dried in air. The electrolyte consisted of 0.1 M phosphate-buffered saline (PBS, pH=7.0) was saturated with nitrogen for 30 minutes before the test. In the control experiment, same amount of nanowires, nanorings and clusters were loaded on electrodes following the same experimental procedure.

Characterization
FTIR spectrometry was performed on a Nicolet AVATAR 360ESP FTIR. The ^{31}P NMR spectrum was obtained by using a JEOL ECA-600 NMR spectrometer (600 MHz, acetone). ICP Elemental analysis of Eu, P and W in the solid samples were determined by inductively coupled plasma atomic emission spectrometry (ICP-AES) (IRIS Intrepid II XSP, ThermoFisher). Elemental analysis of C and H in the solid samples were carried out on a VarioEL (ElementarAnalysensystemeGmbH). The

morphologies of products were carried out on a Hitachi H-7700 at 100 kV, a JEOL 2100F HRTEM equipped with energy dispersive X-ray spectroscopy (EDS) at 200 kV. And a high resolution aberration corrected transmission electron microscope JEOL-ARM200F operated at 200kV, was used to perform high-angle annular-dark-field (HAADF) -STEM. The X-ray photoelectron spectroscopy (XPS) results were achieved by ESCALAB 250Xi (Thermo Fisher). The calibrations were done with respect to carbon C1s. X-ray diffraction (XRD) characterization was carried out on a Bruker D8 X-ray diffractometer using Cu Kα radiation (λ = 0.15418 nm).

Method for simulations of molecular models:

All the $P_2W_{17}M$ (M=Zn, La, Ce) clusters structure with and without HAc were calculated by Gaussian 16 package (*40*) using b3lyp functional. Binding energy between HAc and $P_2W_{17}M$ is calculated according to the equation $\Delta E = E_{POM\text{-}HAc} - E_{POM} - E_{HAc}$ under Basis Set Superposition Error(BSSE) correction, where ΔE is the binding energy between POM and HAc, $E_{POM\text{-}HAc}$ is the energy of POM cluster, E_{HAc} is the energy of HAc. Binding energy is lower or higher than 0 represents that the structure is energetically favored or unfavored.

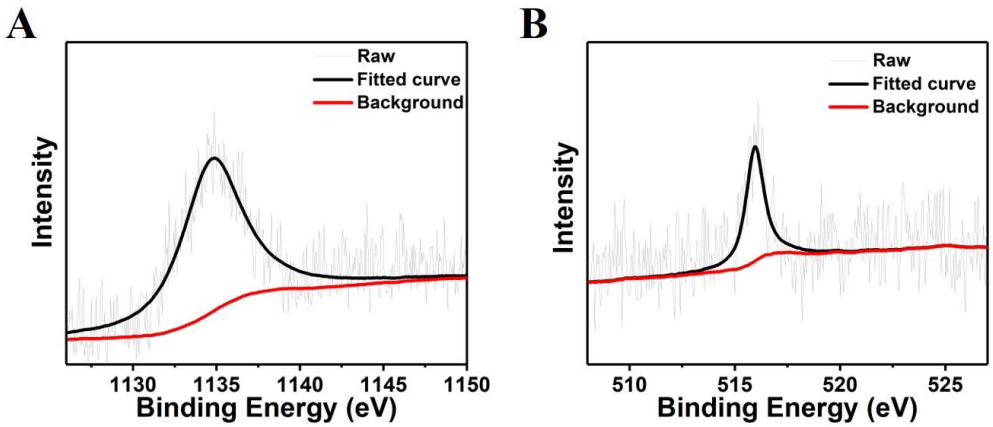

Fig. S1. XPS spectrums of metal elements in nanowire structures. (**A**) Eu 3d5/2. (**B**) V 2p3/2.

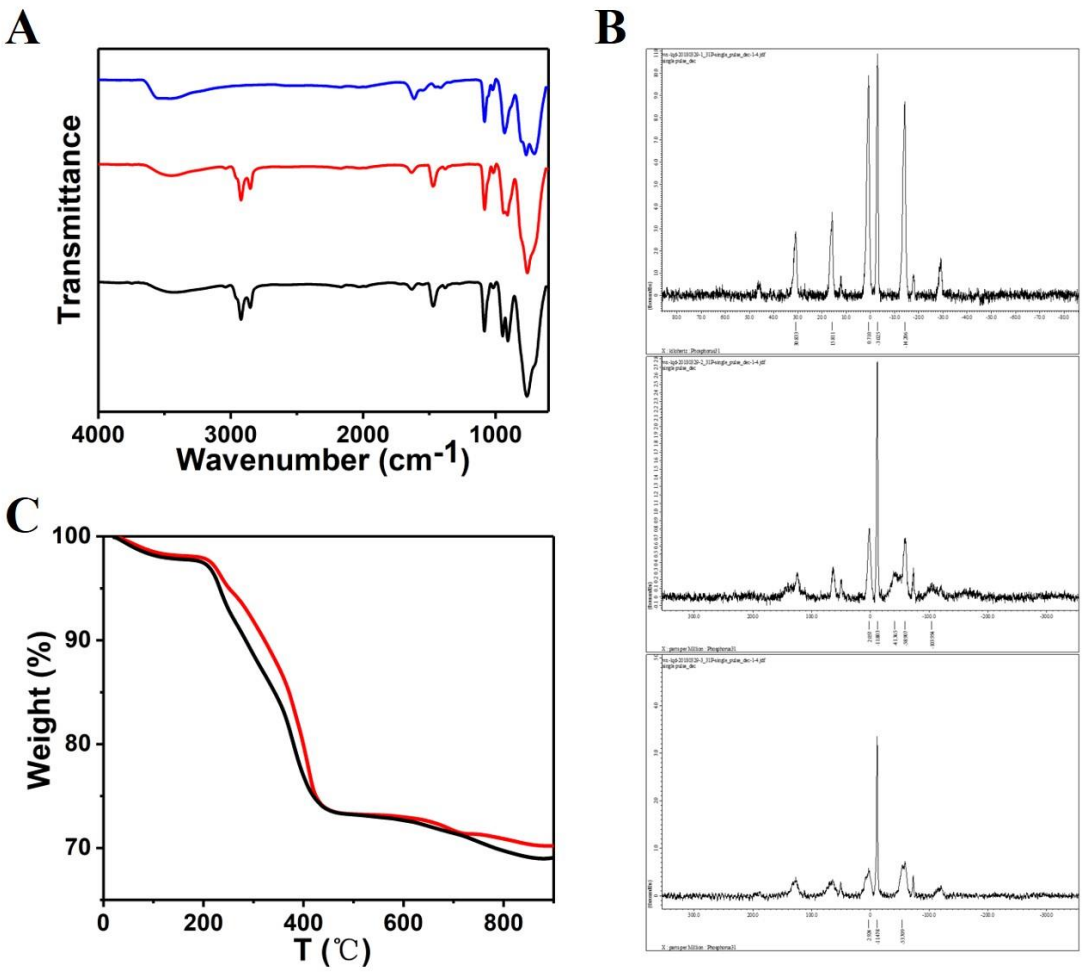

Fig. S2. Characterizations of POM nanowire and nanoring structures. (**A**) FTIR spectra of pure $K_7P_2W_{17}EuO_{61}$ (blue line), POM nanowires (red line) and POM nanorings (black line). (**B**) ^{31}P NMR characterization of pure $K_7P_2W_{17}EuO_{61}$ (top), POM nanowires (central) and POM nanorings (bottom). (**C**) TGA (thermogravimetric analysis) results of nanowire structure (black line) and nanoring structure (red line).

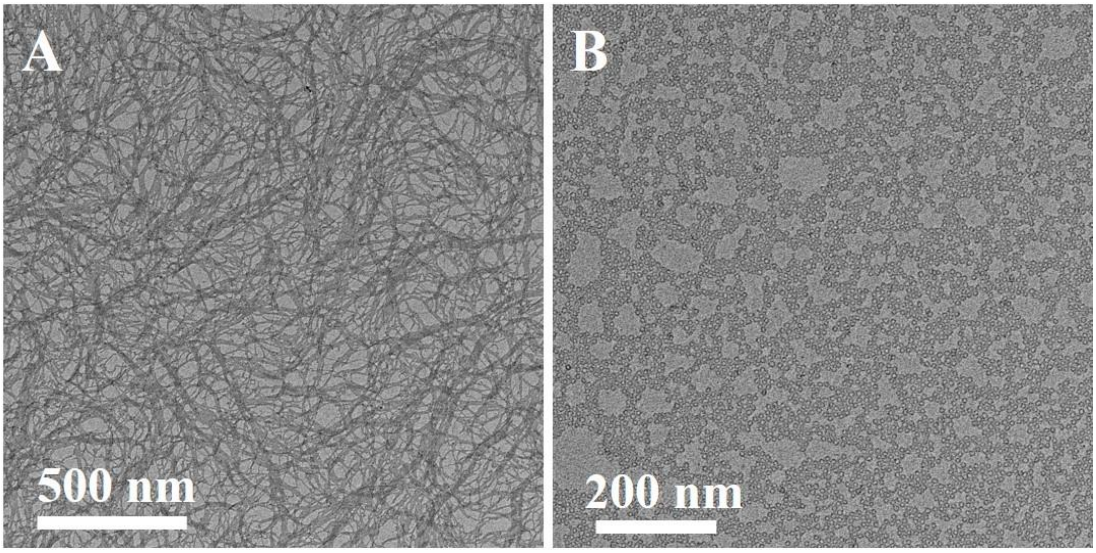

Fig. S3. TEM images of single-cluster nanostructures in low magnification.
(**A**) nanowire structure. (**B**) nanoring structure.

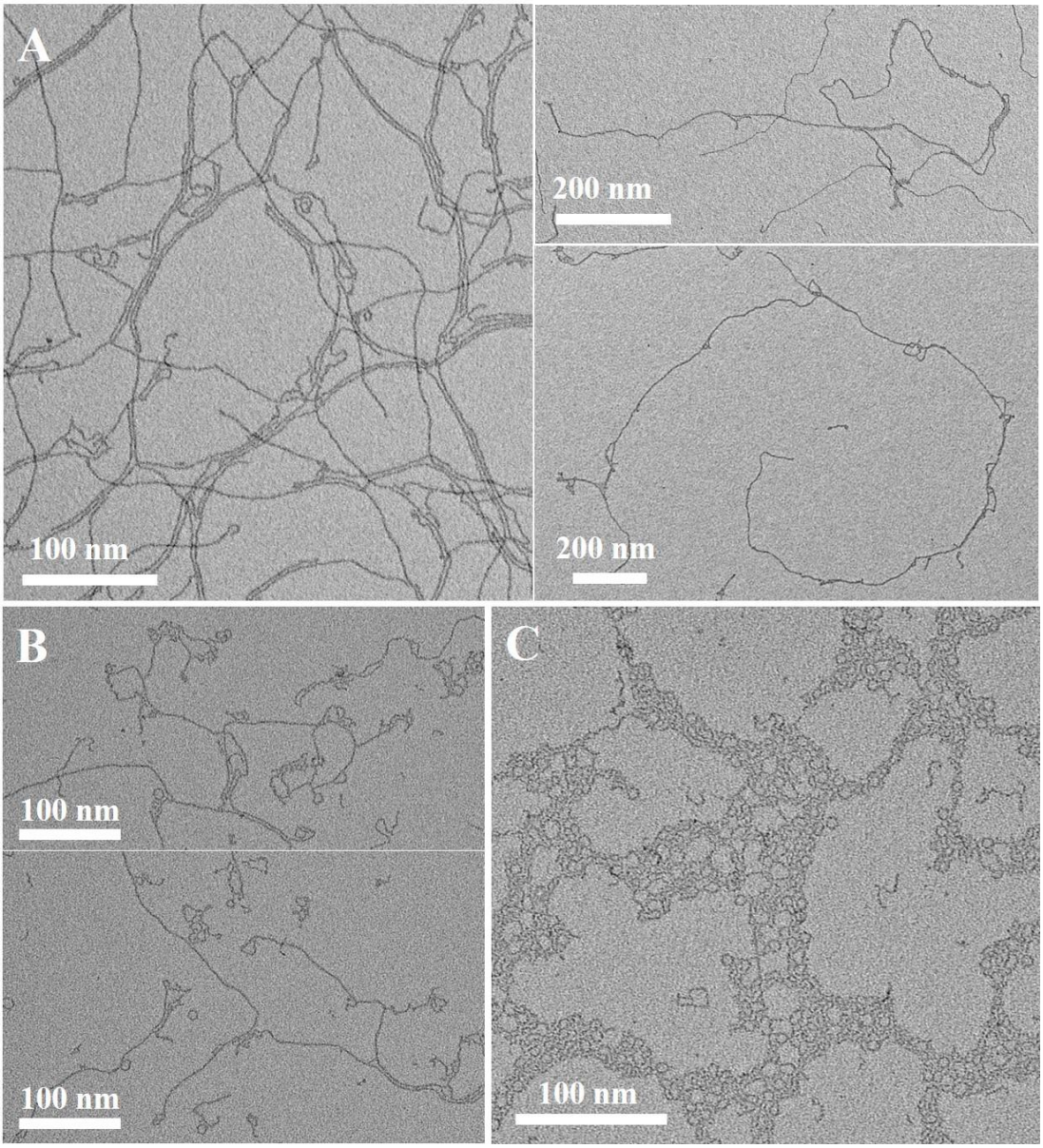

Fig. S4. The morphology transformation from nanowires into nanorings.
(**A**)TEM images of nanowires in diluted solution. (**B**) TEM images of the morphology synthesized in pH=5.0 for 1 h. (**C**) TEM images of the morphology synthesized in pH=4.0 for 1 h.

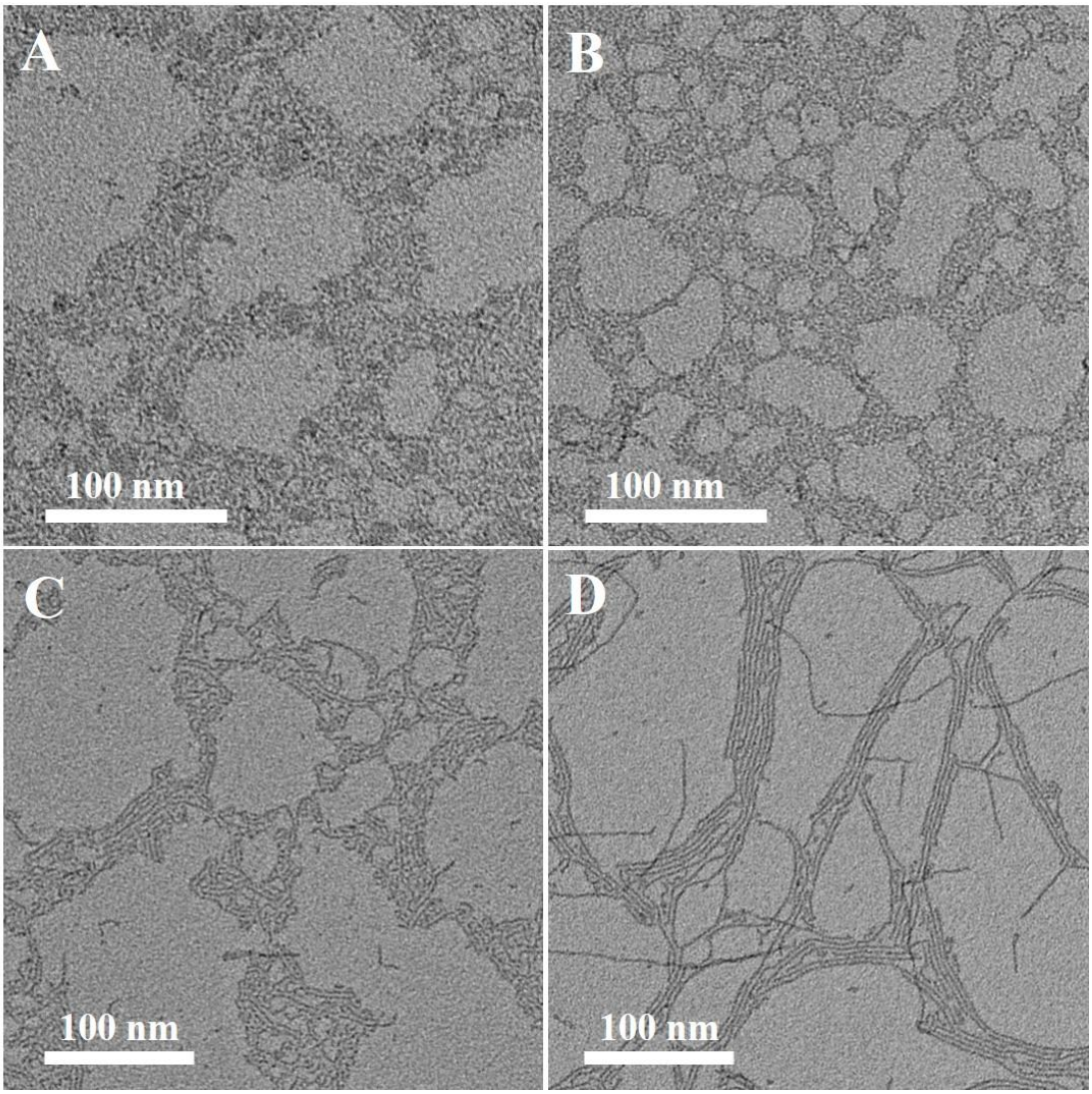

Fig. S5. TEM images of products synthesized with different concentrations of KAc. (**A**) 0 mM KAc. (**B**) 5 mM KAc. (**C**) 10 mM KAc. (**D**) 20 mM KAc.

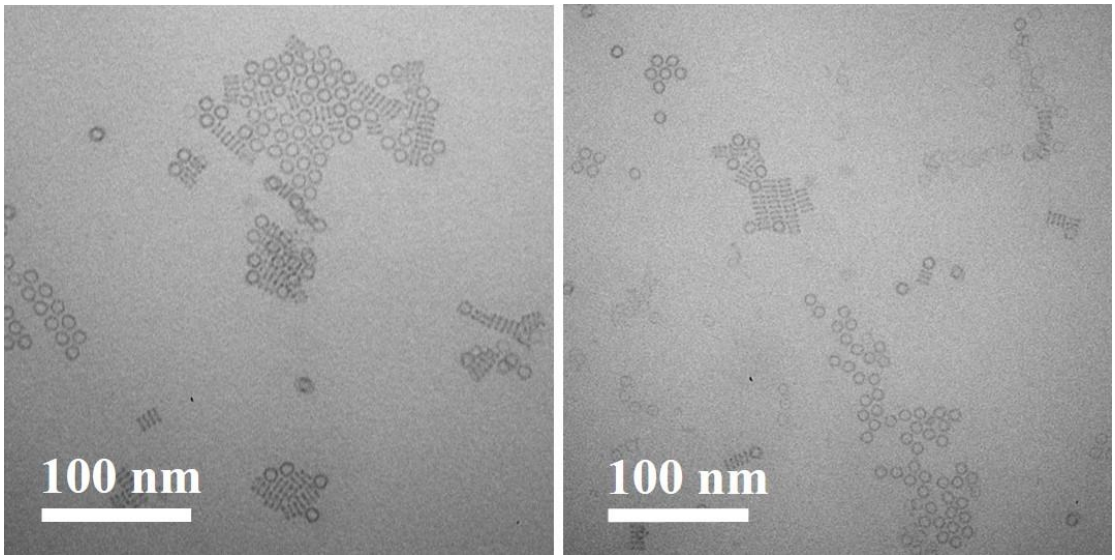

Fig. S6. TEM images of nanocolumns assembled by nanorings.

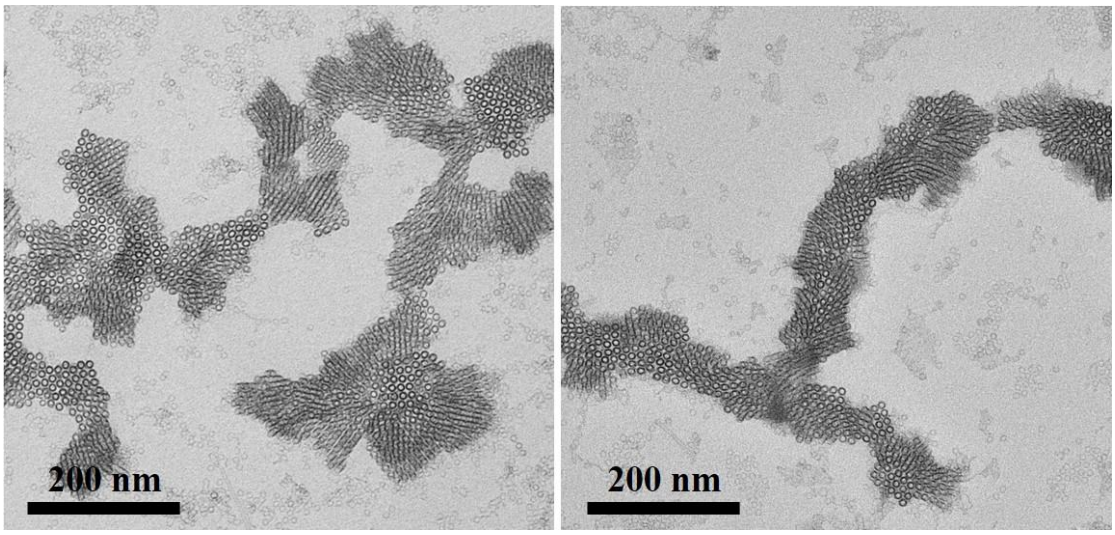

Fig. S7. Typical TEM images of simple cubic $(CTA)_x(TBA)_{7-x}P_2W_{17}EuO_{61}$ superstructures.

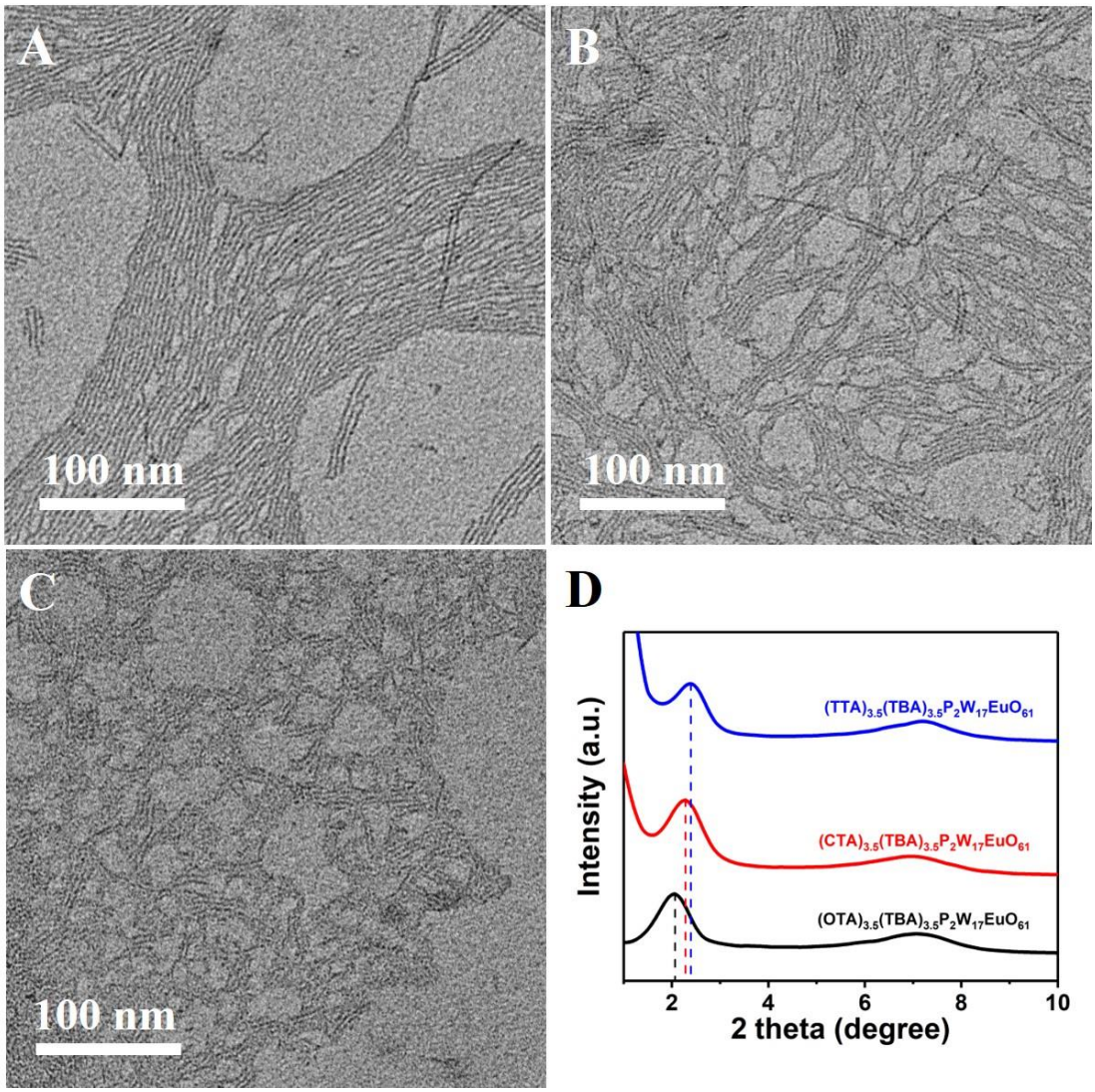

Fig. S8. TEM images of nanowires encapsulated by surfactants with different alkyl chain lengths. (**A**) $(OTA)_x(TBA)_{7-x}P_2W_{17}EuO_{61}$ nanowires. (**B**) $(TTA)_x(TBA)_{7-x}P_2W_{17}EuO_{61}$ nanowires. (**C**) $(DTA)_x(TBA)_{7-x}P_2W_{17}EuO_{61}$ nanowires. (**D**) SAXS patterns of $(OTA)_x(TBA)_{7-x}P_2W_{17}EuO_{61}$ nanowires(black), $(CTA)_x(TBA)_{7-x}P_2W_{17}EuO_{61}$ nanowires (red) and $(TTA)_x(TBA)_{7-x}P_2W_{17}EuO_{61}$ nanowires (blue).

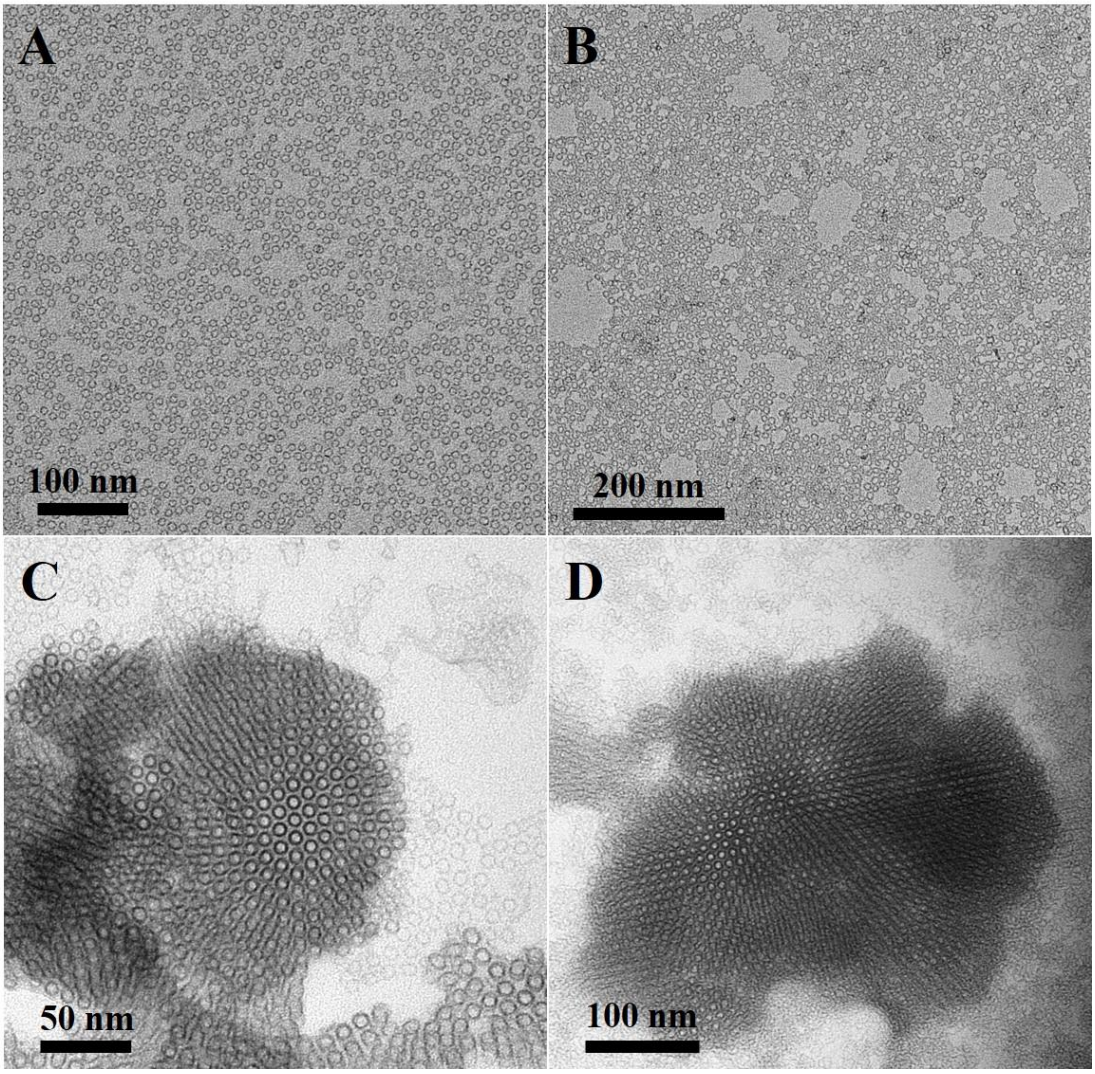

Fig. S9. TEM images of nanorings and 3D superstructures encapsulated by surfactants with different alkyl chain lengths. (**A**) $(OTA)_x(TBA)_{7-x}P_2W_{17}EuO_{61}$ nanorings. (**B**) $(TTA)_x(TBA)_{7-x}P_2W_{17}EuO_{61}$ nanorings. (**C**) $(OTA)_x(TBA)_{7-x}P_2W_{17}EuO_{61}$ 3D superstructures. (**D**) $(TTA)_x(TBA)_{7-x}P_2W_{17}EuO_{61}$ 3D superstructures.

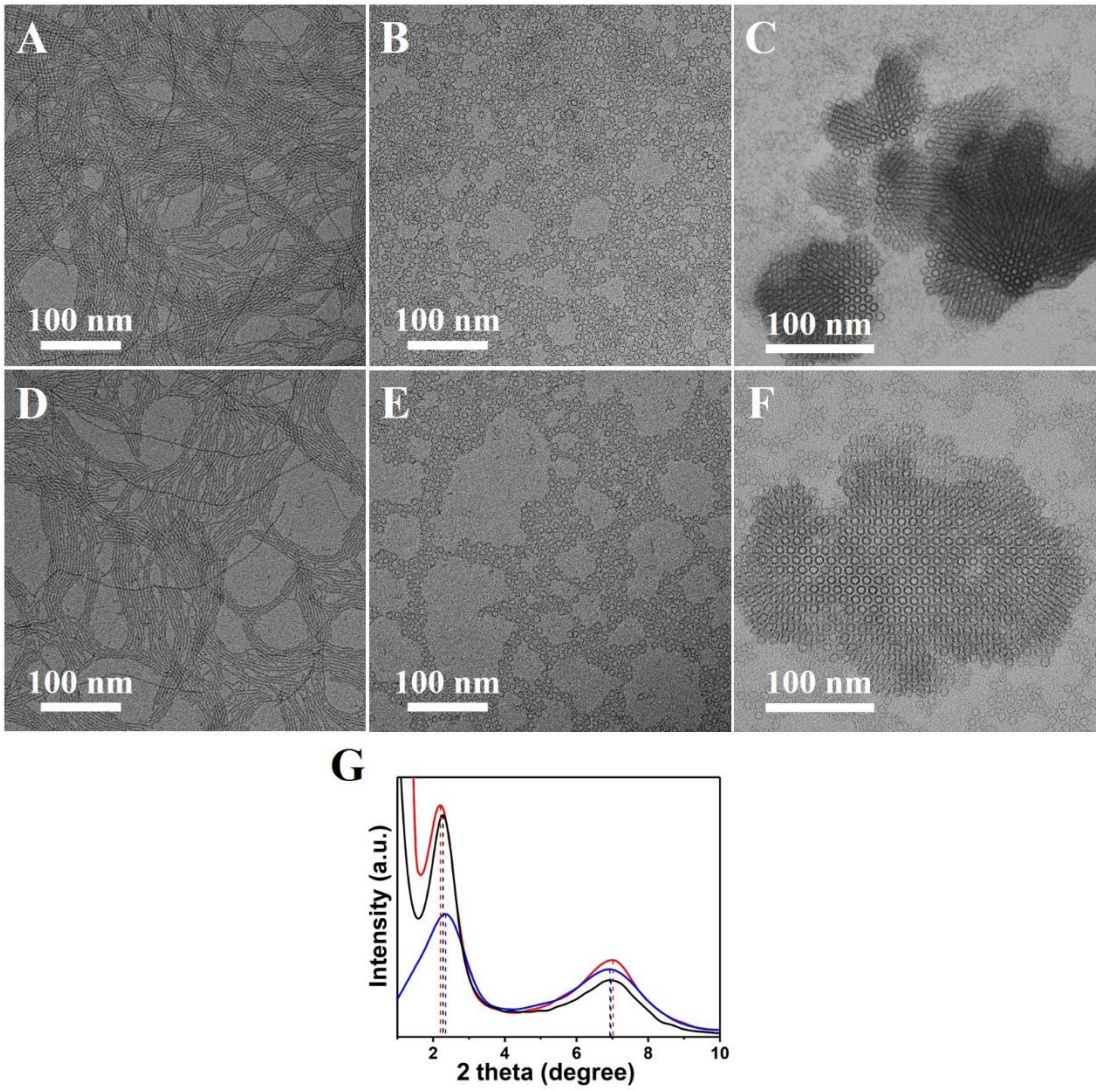

Fig. S10. TEM images of nanowires, nanorings, and 3D superstructures with different alkyl chains of acids. (**A**) nanowires with formates. (**B**) nanorings with formate. (**C**) 3D superstructures with formate. (**D**) nanowires with propionate. (**E**) nanorings with propionate. (**F**) 3D superstructures with propionate. (**G**) SAXS patterns of nanowire structure of formate (red), acetate (black) and propionate (blue).

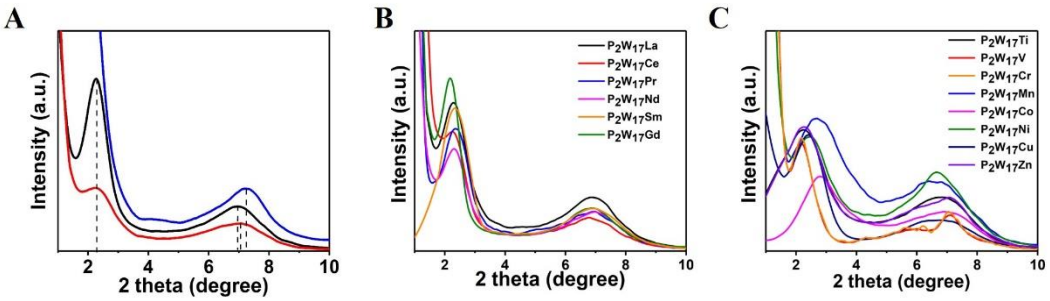

Fig. S11. SAXS results of $P_2W_{17}M$ cluster nanostructures. (**A**) $P_2W_{17}Eu$ nanowire (black), nanoring (red) and 3D superstructure (blue). (**B**) $P_2W_{17}M_{trans}$ cluster nanowires. (**C**) $P_2W_{17}Ln$ cluster nanowires.

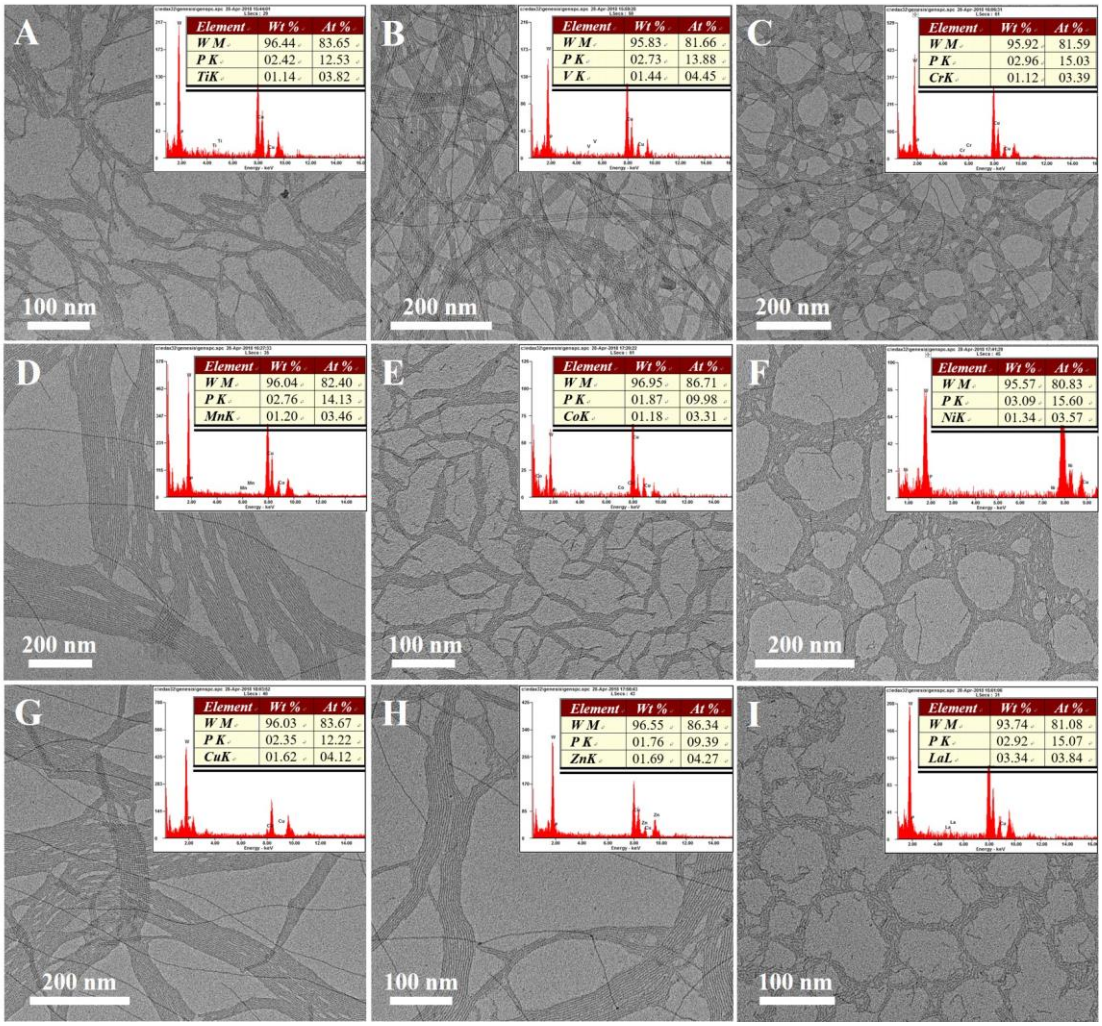

Fig. S12. TEM images and EDX results of nanowire structures constructed by $P_2W_{17}M$ clusters. (**A**) $(CTA)_x(TBA)_{8-x}P_2W_{17}TiO_{61}$ nanowire. (**B**) $(CTA)_x(TBA)_{8-x}P_2W_{17}VO_{62}$ nanowire. (**C**) $(CTA)_x(TBA)_{7-x}P_2W_{17}CrO_{61}$ nanowire. (**D**) $(CTA)_x(TBA)_{8-x}P_2W_{17}MnO_{61}$ nanowire. (**E**) $(CTA)_x(TBA)_{8-x}P_2W_{17}CoO_{61}$ nanowire. (**F**) $(CTA)_x(TBA)_{8-x}P_2W_{17}NiO_{61}$ nanowire. (**G**) $(CTA)_x(TBA)_{8-x}P_2W_{17}CuO_{61}$ nanowire. (**H**) $(CTA)_x(TBA)_{8-x}P_2W_{17}ZnO_{61}$ nanowire. (**I**) $(CTA)_x(TBA)_{7-x}P_2W_{17}LaO_{61}$ nanowire.

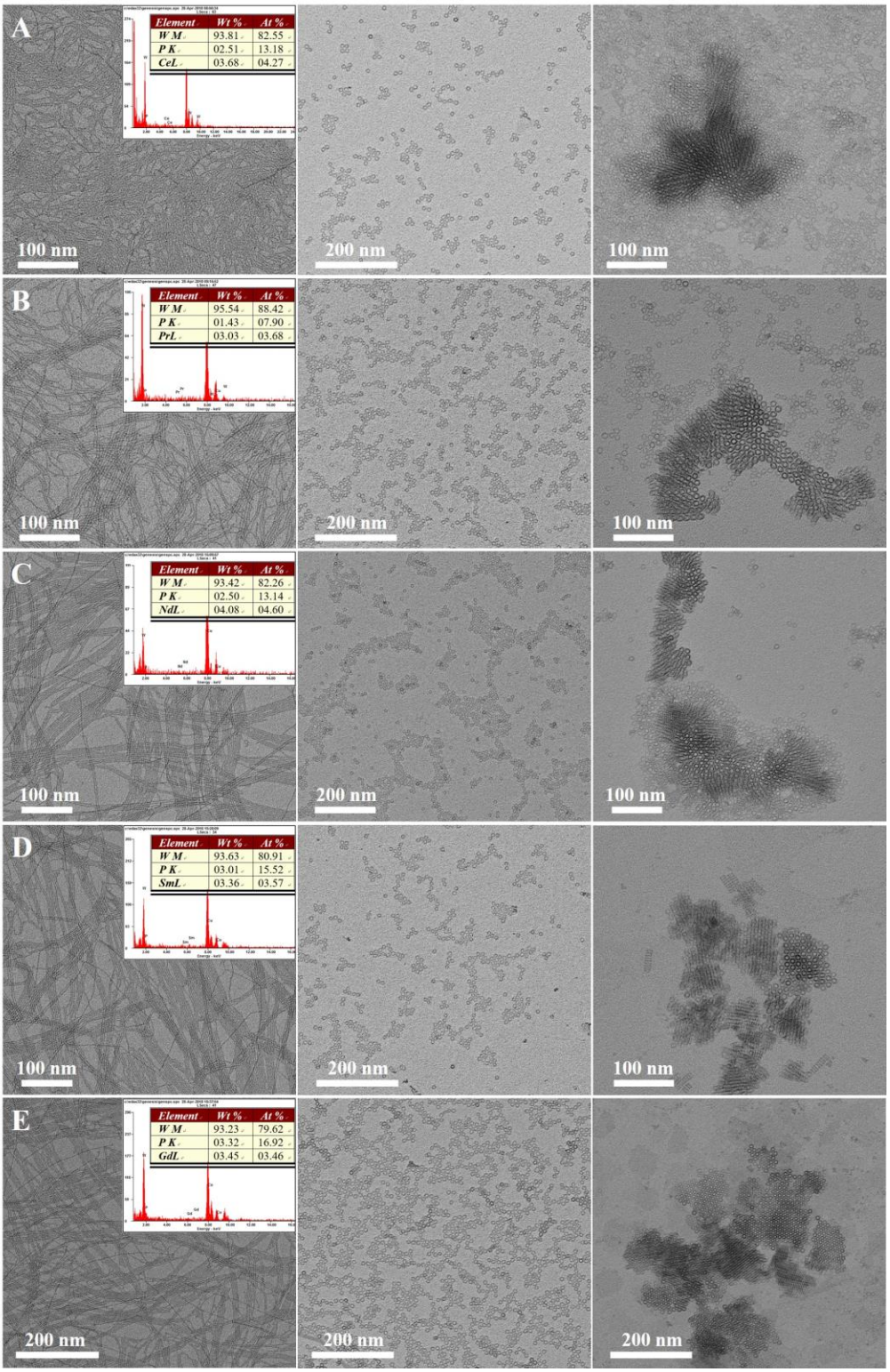

Fig. S13. TEM images and EDX results of nanostructures constructed by $P_2W_{17}Ln$ clusters. (**A**) $(CTA)_x(TBA)_{7-x}P_2W_{17}CeO_{61}$ nanowire, nanoring and 3D superstructures. (**B**) $(CTA)_x(TBA)_{7-x}P_2W_{17}PrO_{61}$ nanowire, nanoring and 3D superstructures. (**C**) $(CTA)_x(TBA)_{7-x}P_2W_{17}NdO_{61}$ nanowire, nanoring and 3D superstructures. (**D**) $(CTA)_x(TBA)_{7-x}P_2W_{17}SmO_{61}$ nanowire, nanoring and 3D superstructures. (**E**) $(CTA)_x(TBA)_{7-x}P_2W_{17}GdO_{61}$ nanowire, nanoring and 3D superstructures.

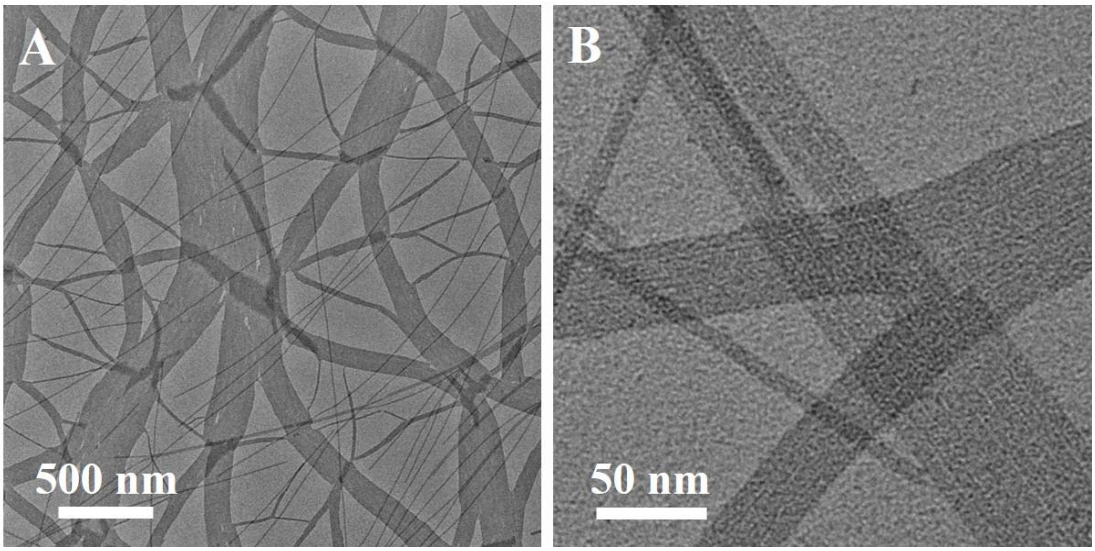

Fig. S14. TEM images of $(CTA)_x(TBA)_{10-x}P_2W_{17}O_{61}$ nanobelts. (**A**) Low magnification image. (**B**) High magnification image.

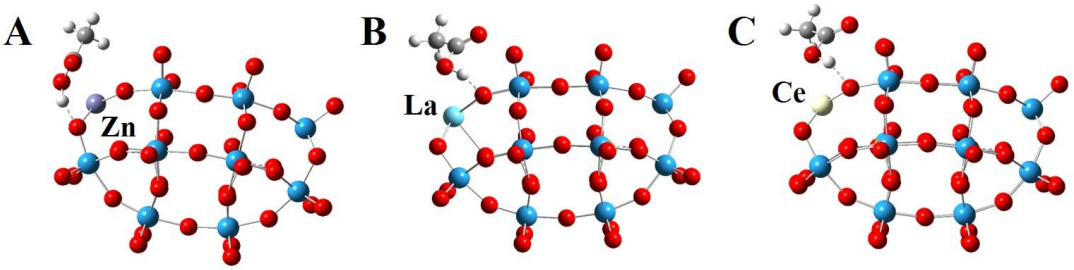

Fig. S15. Optimized complex structure of HAc and the $P_2W_{17}M$ (M = Zn, La, Ce) cluster. (**A**) Zn. (**B**) La. (**C**) Ce.

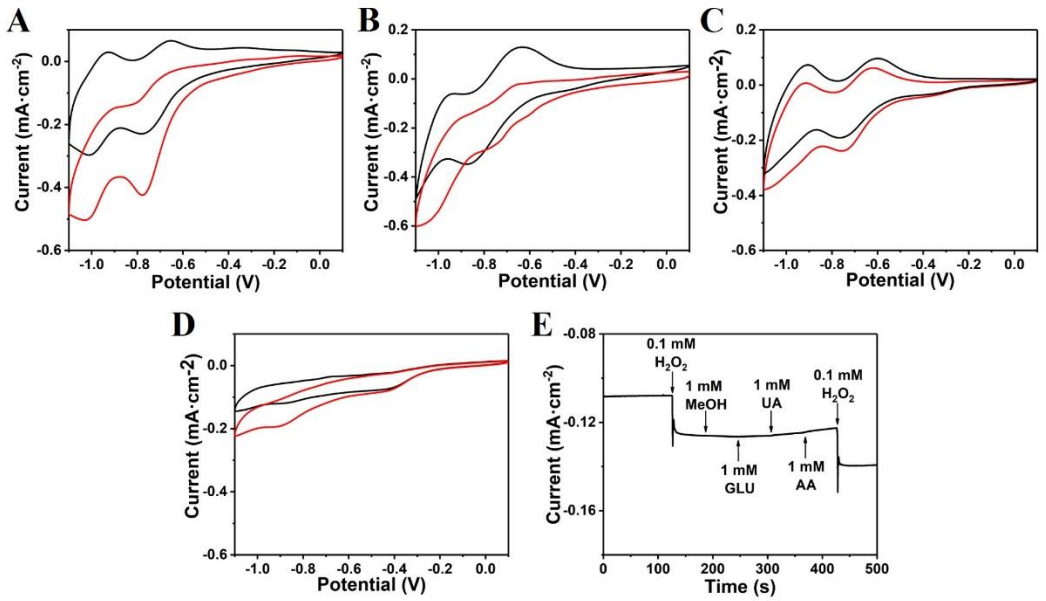

Fig. S16. CV curves and selectivity test for the hydrogen peroxide detection. CV curves of (**A**) 3D superstructure, (**B**) nanoring, (**C**) nanowire, (**D**) POM cluster in nitrogen saturated 0.1 M PBS without H_2O_2 (black line) and with 2 mM H_2O_2 (red line) at a scan rate of 50 mV s^{-1}. (**E**) Amperometric response of 3D superstructure with successive addition of 0.1 mM H_2O_2, 1 mM methol, 1 mM glucose, 1 mM uric acid, 1 mM ascorbic acid and 0.1 mM H_2O_2 at -0.78 V vs.SCE.

Table S1. Elemental analysis results of nanowire and nanoring structures.

Sample	C	H	P	W	Eu
Nanowire	25.21	5.44	0.90	46.71	2.01
Nanoring	25.02	5.40	0.91	47.22	2.07
Calcd for $(CTA)_{3.5}(TBA)_{3.5}P_2W_{17}EuO_{61}$	23.88	4.47	1.01	50.74	2.47

Table S2. Epoxidation of olefins with PhIO catalyzed by the $P_2W_{17}Mn$ POM precursor.

Entry	Alkene	Yield of epoxide [%]
1	cyclooctene	64
2	cyclohexene	60
3	cis-3-hexene	67
4	styrene	66